Front. Phys. 13(4), 138117 (2018)
https://doi.org/10.1007/s11467-018-0810-2

RESEARCH ARTICLE

Monolayered semiconducting GeAsSe and SnSbTe with ultrahigh hole mobility

Yu Guo[1,2], Nan Gao[1], Yizhen Bai[1], Jijun Zhao[1,†], Xiao Cheng Zeng[2,3,‡]

[1] *Key Laboratory of Materials Modification by Laser, Ion and Electron Beams (Dalian University of Technology), Ministry of Education, Dalian 116024, China*
[2] *Department of Chemistry, University of Nebraska–Lincoln, Lincoln, NE 68588, USA*
[3] *Department of Chemical & Biomolecular Engineering and Department of Mechanical & Materials Engineering, University of Nebraska–Lincoln, Lincoln, NE 68588, USA*
Corresponding authors. E-mail: [†] *zhaojj@dlut.edu.cn,* [‡] *xzeng1@unl.edu*
Received June 10, 2018; accepted June 24, 2018

High carrier mobility and a direct semiconducting band gap are two key properties of materials for electronic device applications. Using first-principles calculations, we predict two types of two-dimensional semiconductors, ultrathin GeAsSe and SnSbTe nanosheets, with desirable electronic and optical properties. Both GeAsSe and SnSbTe sheets are energetically favorable, with formation energies of −0.19 and −0.09 eV/atom, respectively, and have excellent dynamical and thermal stability, as determined by phonon dispersion calculations and Born–Oppenheimer molecular dynamics simulations. The relatively weak interlayer binding energies suggest that these monolayer sheets can be easily exfoliated from the bulk crystals. Importantly, monolayer GeAsSe and SnSbTe possess direct band gaps (2.56 and 1.96 eV, respectively) and superior hole mobility ($\sim$ 20 000 cm^2·V^{-1}·s^{-1}), and both exhibit notable absorption in the visible region. A comparison of the band edge positions with the redox potentials of water reveals that layered GeAsSe and SnSbTe are potential photocatalysts for water splitting. These exceptional properties make layered GeAsSe and SnSbTe promising candidates for use in future high-speed electronic and optoelectronic devices.

Keywords 2D GeAsSe and SnSbTe, carrier mobility, photocatalysts, DFT calculations

PACS numbers 73.21.At, 73.22.-f, 81.07.-b, 88.80.-q

1 Introduction

Two-dimensional (2D) layered materials with atomic thickness, such as graphene, silicene, phosphorene, and transition-metal dichalcogenides, have attracted extensive interest because of their intriguing physical and chemical properties and potential applications in future electronics and optoelectronics devices [1–4]. Graphene has been the most widely studied 2D material. However, the gapless nature of graphene limits its practical applications in high-speed switching devices or photocatalysts [5]. Transition-metal dichalcogenide monolayers possess moderate band gaps suitable for field-effect transistors, but their relatively low carrier mobilities are not as competitive as those of the commonly used silicon [6, 7]. Phosphorene has a suitable band gap and high carrier mobility [8]; however, phosphorus-based 2D materials are unstable in air and tend to degrade very rapidly in ambient air [9, 10]. It is thus desirable to explore novel 2D semiconductors with high carrier mobility, a moderate direct band gap, and excellent stability.

Very recently, various ultrathin chalcogenide sheets with superior chemical and physical properties have been successfully synthesized [11–16]. For instance, group-III and group-IV monochalcogenide monolayers exhibited excellent air stability and high mobilities of up to 12 700 cm^2·V^{-1}·s^{-1} [17–20]. Stable ternary bismuth chalcogenide films [16], such as Bi_2O_2Se, have a band gap of ∼0.8 eV and a high electron mobility of ∼ 29 000 cm^2·V^{-1}·s^{-1} at 1.9 K [21–24]. A ternary $MnPSe_3$ monolayer exhibits strong absorption in the visible region, photocatalytic activity for water splitting, and modest carrier mobility (625.9 cm^2·V^{-1}·s^{-1}) [25, 26]. Note that

*Special Topic: Graphene and other Two-Dimensional Materials (Eds. Daria Andreeva, Wencai Ren, Guangcun Shan & Kostya Novoselov).

© Higher Education Press and Springer-Verlag GmbH Germany, part of Springer Nature 2018

as a nanomaterial, GeAsSe is a semiconductor with a moderate band gap of approximately 2.26 eV [27], which is suitable for optoelectronic applications such as optical amplification [28], nonlinear directional coupler switch [29], and refractive index sensing [30]. Further, GeAsSe is a layered crystal with weak interlayer interaction [31], indicating that monolayer exfoliation from the bulk is experimentally feasible. By using the strategy of atomic transmutation [32], it should be possible to fabricate a hypothetical SnSbTe structure that is similar to that of GeAsSe, because the elements Sn and Ge, Sb and As, and Te and Se belong to the same groups in the periodic table.

In this work, our first-principles calculations predict that monolayer GeAsSe and SnSbTe can possibly be exfoliated from their layered bulk counterparts, like graphene [33, 34]. Both GeAsSe and SnSbTe monolayers exhibit excellent thermal and dynamical stability. More importantly, layered GeAsSe and SnSbTe are predicted to have a moderate band gap and ultrahigh hole mobility, and their optical absorption spectra cover nearly the entire incident solar spectrum. The band edge positions calculated using the accurate HSE06 functional indicate that layered GeAsSe and SnSbTe could be efficient catalysts for photocatalytic splitting of water. All these results suggest excellent opportunities for future (opto)electronic applications.

2 Computational methods

Density functional theory (DFT) calculations were performed using the Vienna *ab initio* simulation package (VASP 5.4) [35], using the plane-wave basis set with a cutoff of 500 eV, the projector augmented wave potentials [35, 36], and the generalized gradient approximation (GGA) parameterized by Perdew, Burke and Ernzerhof (PBE) [37] for the exchange-correlation functional. The convergence criterion for the total energy was set to 10^{-7} eV. The geometry optimization was considered to be converged when the residual force on each atom was less than 0.01 eV·Å^{-1}. Uniform k-point meshes with a spacing of ~0.015 Å^{-1} were adopted to sample the Brillouin zone of the unit cells [38]. A vacuum region of 20 Å was added in the vertical direction to avoid interactions between neighboring layers. Note that the standard GGA functionals tend to underestimate the band gap of a semiconductor; thus, a hybrid functional (HSE06) [39, 40] was also used to compute the electronic band structures of monolayer GeAsSe and SnSbTe with the optimized geometries. The Grimme's semi-empirical DFT-D3 method [41] was adopted to describe the long-range van der Waals (vdW) interactions. Phonon dispersion analysis was performed using the Phonopy code based on density functional perturbation theory as implemented in VASP [42]. Born–Oppenheimer molecular dynamics (BOMD) simulations [43] using the PBE functional were conducted to assess the thermal stability of these monolayers. In the BOMD simulations, the initial configuration of monolayers with a 4 × 2 × 1 supercell was annealed under several selected temperatures. Each BOMD simulation in the NVT ensemble lasted for 10 ps with a time step of 1.0 fs, and the temperature was controlled by the Nosé-Hoover method [44].

3 Results and discussion

As shown in Fig. 1, monolayer GeAsSe and SnSbTe possess networks of puckered orthorhombic structures in the xy plane. The structural parameters are given in Table 1. The puckered structures yield larger lattice constants along the y direction than along the x direction. Monolayer GeAsSe has smaller lattice constants (5.14 Å along

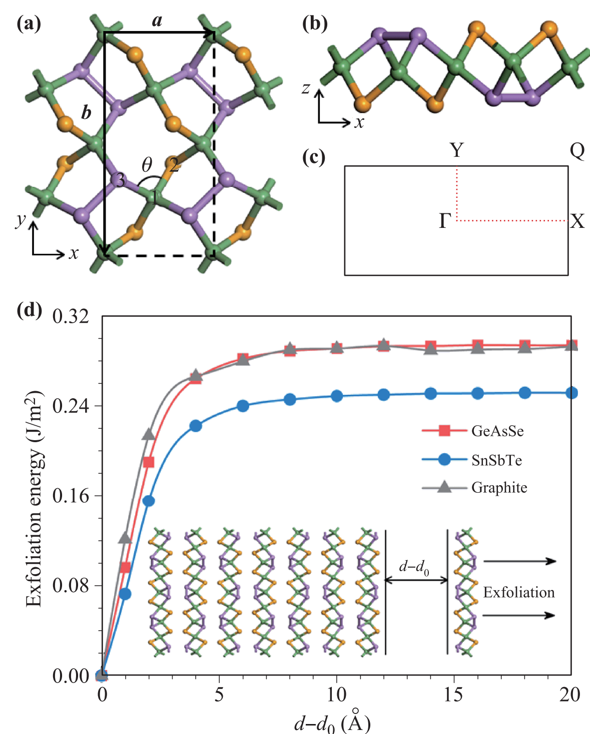

Fig. 1 **(a, b)** are top and side views of the atomic structures of monolayer GeAsSe or SnSbTe. The unit cell is denoted by dashed lines. ***a*** and ***b*** represent the lattice constant along x and y direction, respectively. The 2D Brillouin zone is shown in **(c)**, with high-symmetry points labeled. **(d)** Exfoliation energy vs. separation distance d for monolayer GeAsSe and SnSbTe in comparison with graphite, where d_0 indicates the van der Waals distance between adjacent layers in the bulk crystal. The green, purple and orange balls represent Ge/Sn, As/Sb and Se/Te, respectively.

Table 1 Lattice constant (a, b), bond lengths of Ge-Se/Sn-Te (l_{1-2}) and Ge-As/Sn-Sb (l_{1-3}) and the angle (θ) of As-Ge-Se/Sb-Sn-Te as shown in Fig. 1(a); formation energy of monolayers (ΔH); electronic band gap (E_g); bond overlap population for Ge-Se/Sn-Te and Ge-As/Sn-Sb bonds; The charge transfer from Ge/Sn to As/Sb and Se/Te atoms is also given for the monolayer GeAsSe and SnSbTe by Hirshfeld charge analysis. "1-2" and "1-3" represent the bonds of Ge-Se and Ge-As for monolayer GeAsSe, and Sn-Te and Sn-Sb for monolayer SnSbTe, respectively.

Material	a	b	l_{1-2}	l_{1-3}	θ	ΔH	E_g	Bond population		Charge transfer
	Å				°	eV/atom	eV	1-2	1-3	e
GeAsSe	5.14	10.40	2.39	2.52	114.77	−0.19	2.56	0.48	0.40	0.12
SnSbTe	5.87	11.89	2.78	2.89	113.82	−0.09	1.96	0.55	0.49	0.13

the x direction and 10.40 Å along the y direction) than monolayer SnSbTe (5.87 Å along the x direction and 11.89 Å along the y direction). Population analysis [45] reveals that monolayer GeAsSe is made of covalent bonds with a bond overlap population of 0.48 for Ge–Se bonds and 0.40 for Ge–As bonds, accompanied by a prominent charge transfer of 0.12e from Ge to As and Se. Monolayer SnSbTe holds an even larger bond overlap population (0.55 for Sn–Te bonds and 0.49 for Sn–Sb bonds) and charge transfer (0.13e from Sn to Sb and Te). As shown in Fig. 1, bulk GeAsSe is a natural pseudo-2D crystal [31] possessing planar 2D networks of puckered orthorhombic structures in the xy plane and vdW interlayer stacking along the z direction. Hypothetically, SnSbTe might possess a structure analogous to that of GeAsSe. Furthermore, to examine the possibility of fabricating monolayers from the layered crystal, we simulated the exfoliation process and predicted the exfoliation energy with respect to the separation distance, as shown in Fig. 1(d). The calculated exfoliation energy of graphite is 0.30 J·m^{-2}, which is consistent with an experimental measurement (0.32±0.03 J·m^{-2}) [34] and a previous theoretical value (0.32 J·m^{-2}) [33]. For monolayer GeAsSe and SnSbTe, the calculated exfoliation energies are 0.29 and 0.25 J·m^{-2}, respectively, which are slightly smaller than that of graphite. Hence, like graphene, monolayer GeAsSe and SnSbTe can be prepared experimentally from their bulk forms by mechanical cleavage or liquid-phase exfoliation.

The stability of a 2D crystal is crucial for experimental fabrication and practical applications. To evaluate the energetic stability of monolayer GeAsSe and SnSbTe, we first calculated the formation energy ΔH, which is defined as

$$\Delta H = (E_{\text{tot}} - n_1 \times E_1 - n_2 \times E_2 - n_3 \times E_3)/n, \quad (1)$$

where E_{tot} is the total energy of monolayer GeAsSe (SnSbTe), and E_1, E_2, and E_3 are the energies per atom in Ge (Sn), As (Sb), and Se (Te) solids, respectively. The factors n_1, n_2, and n_3 denote the number of Ge (Sn), As (Sb), and Se (Te) atoms in the unit cell, respectively, and the factor n represents the total number of atoms in the unit cell. The calculated ΔH is −0.19 eV/atom for monolayer GeAsSe and −0.09 eV/atom for monolayer SnSbTe, which are comparable to those of successfully synthesized materials such as layered GeAs (−0.075 eV/atom) [46] and GaTe (−0.37 eV/atom) [15]. The relatively low formation energies reveal that the formation of monolayer GeAsSe and SnSbTe is exothermic. The lattice dynamical stability of monolayer GeAsSe and SnSbTe is assessed by calculating the phonon dispersion curves, as shown in Fig. 2(a). No imaginary phonon mode is observed, indicating that the 2D GeAsSe and SnSbTe crystals are dynamically stable. We also performed BOMD simulations

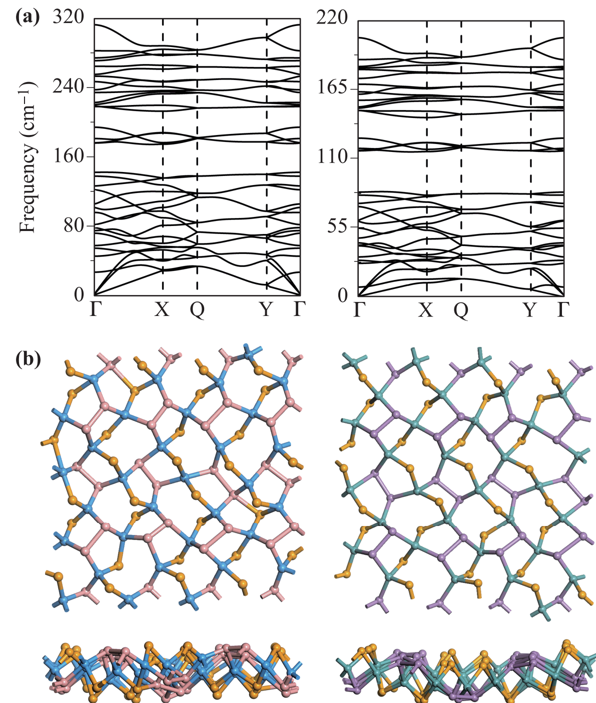

Fig. 2 **(a)** Phonon dispersions of monolayer GeAsSe (left panel) and SnSbTe (right panel). **(b)** Snapshots of the equilibrium structures of monolayer GeAsSe at 1400 K (left panel) and SnSbTe at 900 K (right panel) after 10 ps Born-Oppenheimer molecular dynamic simulation. Ge, As, Se, Sn, Sb and Te atoms are shown in blue, pink, orange, green, purple and yellow colors, respectively.

Frontiers of Physics

to examine the thermal stability of these 2D structures at elevated temperature. Even up to 1400 K (900 K), monolayer GeAsSe (SnSbTe) can maintain its structural integrity for at least 10 ps [Fig. 2(b)], indicating superior stability above room temperature. At 1500 K for monolayer GeAsSe and 1000 K for monolayer SnSbTe, the planar structures are highly distorted after 10 ps of BOMD simulation (Fig. A1).

The electronic band structure and local density of states (LDOS) of monolayer GeAsSe and SnSbTe are computed using the HSE06 functional (Fig. 3). Monolayer GeAsSe and SnSbTe possess finite direct band gaps of 2.56 eV and 1.96 eV at the Γ point, respectively. Taking monolayer GeAsSe as representative, the LDOS analysis reveals that the top valence bands stem mainly from the 4p orbitals of Se atoms and partially from the 4p orbitals of Ge and As atoms, whereas the 4p orbitals of Ge, As, and Se atoms together contribute to the bottom conduction bands. The LDOS of monolayer SnSbTe exhibits behavior similar to that of monolayer GeAsSe. Further, the substantial overlap of the LDOS near the Fermi level implies strong hybridization between the orbitals of Ge, As, and Se atoms. The effective masses of electrons (m_e) and holes (m_h) are calculated by fitting parabolic functions to the conduction band minimum (CBM) and valence band maximum (VBM), respectively. The computed carrier effective masses are generally in the range of $0.41m_0$–$4.69m_0$ (m_0 is the electron rest mass) for monolayer GeAsSe and $0.42m_0$–$3.43m_0$ for monolayer SnSbTe (see Table 2). In particular, the effective electron mass could be as low as $0.41m_0$ along the y direction, indicating that the carriers in these 2D sheets are rather mobile. Moreover, the large longitudinal/horizontal anisotropy of the mass makes them promising candidates for carrier transport and rectifier devices.

To examine the strain effect on the band gap, we compute the electronic band structures of monolayer GeAsSe and SnSbTe under various uniaxial and biaxial strains up to ±3% (see Fig. A2 for details). The results indicate that the band gap of monolayer GeAsSe (SnSbTe) decreases linearly from 2.76 to 2.39 eV (from 2.07 to 1.83

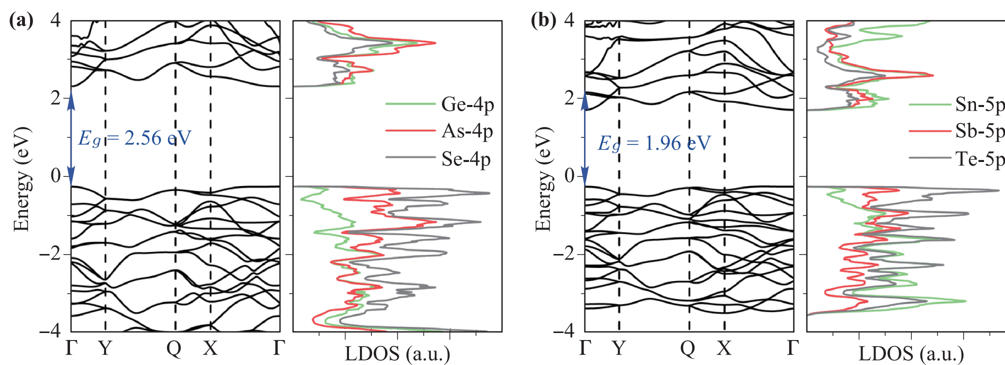

Fig. 3 **(a, b)** are the electronic band structures (left panel) and LDOS (right panel) for monolayer GeAsSe and SnSbTe, respectively. E_g is the band gap denoted by the solid arrow. The representation of high-symmetry points of the first Brillouin zone are illustrated in Fig. 1(c).

Table 2 Calculated carrier effective mass m, elastic modulus C, deformation potential constant (E_1), and carrier mobility (μ) along x and y directions for monolayer GeAsSe and SnSbTe at 300 K. N_L represents the number of layers. m_0 is the electron rest mass.

Material	N_L	Carrier	m_x	m_y	E_{1x}	E_{1y}	C_x	C_y	μ_x	μ_y
			m_0		eV		J·m^{-2}		cm^2·V^{-1}·s^{-1}	
GeAsSe	1	h	4.69	1.39	0.45	0.10	31.53	32.96	275.92	18149.84
		e	2.01	0.41	4.55	5.01	31.53	32.96	17.73	75.59
	2	h	4.17	1.16	1.72	0.99	64.55	65.93	50.32	554.03
		e	2.08	0.49	5.05	5.69	64.55	65.93	25.47	86.77
SnSbTe	1	h	3.43	2.33	0.31	0.05	17.46	18.68	389.31	21308.35
		e	1.39	0.42	4.36	3.66	17.46	18.68	18.39	92.92
	2	h	4.67	2.41	2.01	1.85	45.90	41.05	15.25	31.37
		e	2.16	0.57	5.40	4.18	45.90	41.05	13.80	78.45

eV) under uniaxial strains of −3% to 3%, and from 2.90 to 2.25 eV (from 2.15 to 1.69 eV) under biaxial strains of −3% to 3%. For the multilayer sheets, as the layer thickness increases, the band gap decreases monotonically (see Fig. A3). Consequently, bilayer, trilayer, and bulk GeAsSe preserve their semiconducting behavior, with indirect band gaps of 2.39, 2.30, and 2.15 eV, respectively. For SnSbTe, its bilayer, trilayer, and bulk systems also remain semiconducting, with band gaps of 1.64 eV (indirect), 1.25 eV (direct), and 0.89 eV (direct), respectively.

The band structures and LDOSs from the HSE06 calculations yield band gaps of 2.56 eV for monolayer GeAsSe and 1.96 eV for monolayer SnSbTe, which both exceed the water redox potential (1.23 eV). In addition to a band gap of the appropriate magnitude, band edges that straddle the redox potential of water are necessary for photocatalytic application. For the water splitting reaction, the redox potential depends on the pH [47–50]. The standard reduction potential for H^+/H_2 was calculated as $E_{H+/H2} = -4.44$ eV + pH $\times 0.059$ eV, and the oxidation potential for O_2/H_2O was calculated as $E_{O2/H2O} = -5.67$ eV + pH $\times 0.059$ eV. Figure 4 shows the band alignments of layered GeAsSe and SnSbTe with respect to the redox potential of water splitting at pH = 0 and 7. The calculations show that the band edges of monolayer, bilayer, and trilayer GeAsSe at pH = 0 and 7 all straddle the redox potential of water, indicating that layered GeAsSe is a good candidate for use as a photocatalyst without an external bias voltage in acidic and neutral environments. The band edges of monolayer SnSbTe satisfy the conditions for water splitting at pH values of both 0 and 7. Bilayer SnSbTe is suitable for water splitting in neutral environments, whereas its VBM almost overlaps the oxidation potential of O_2/H_2O at pH = 0. Thus, it has only limited capacity to split water by producing oxygen in an acidic environment. Trilayer SnSbTe may not provide sufficient potential to drive water splitting owing to its small band gap. Therefore, our calculations of the band gaps and band edge positions using the accurate hybrid HSE06 functional predict that layered GeAsSe and monolayer SnSbTe are suitable photocatalysts for water splitting.

Another important requisite for photocatalytic water splitting is that the material should capture a significant fraction of the visible spectrum, which accounts for more than 40% of the solar spectrum [25]. To examine the performance under light, the optical absorption coefficients (defined as the decay of light intensity spreading in a unit length of the medium) of monolayer GeAsSe and SnSbTe are obtained by computing the complex dielectric functions based on the HSE06 functional, as shown in Fig. 5. Monolayer GeAsSe and SnSbTe exhibit obvious optical absorption in the visible spectrum, with an absorption coefficient of up to 10^5 cm^{-1}, which is comparable to those of bulk MoS_2 [$(0.1–0.6) \times 10^6$ cm^{-1}] [51]. These characteristics, along with the direct moderate gaps and favorable band edges, should give monolayer GeAsSe and SnSbTe satisfactory performance for photocatalytic water splitting.

To further evaluate the performance of monolayer GeAsSe and SnSbTe as photocatalysts and electronic materials, their carrier mobility μ is calculated for quantitative evaluation of the electron/hole transport along specific directions. On the basis of the Takagi model within the deformation potential approximation [52–54], the acoustic phonon-limited carrier mobility μ can be derived as

$$\mu = \frac{e\hbar^3 C_{2D}}{k_B T m m_d (E_{1,i})^2}, \tag{2}$$

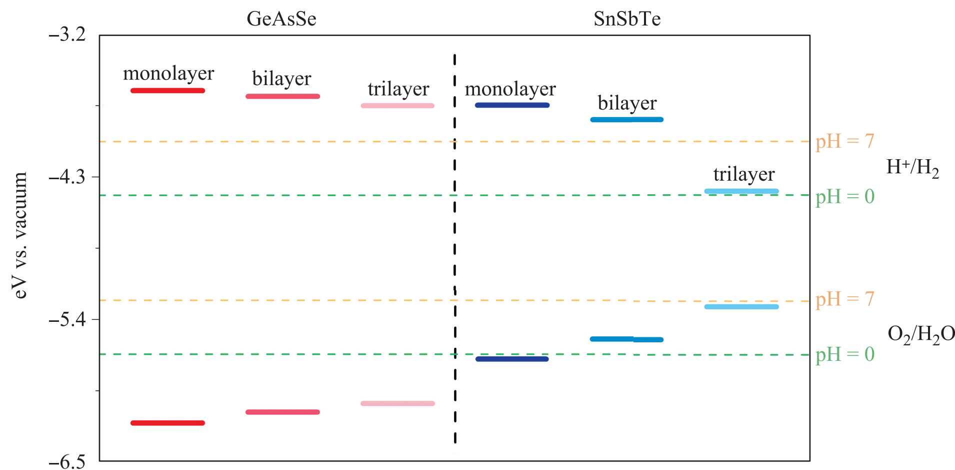

Fig. 4 The location of VBM and CBM relative to vacuum energy calculated with HSE06 functional of monolayer, bilayer and trilayer GeAsSe and SnSbTe. The redox potentials of water splitting at pH = 7 (orange dashed lines) and pH = 0 (green dashed lines) are shown for comparison.

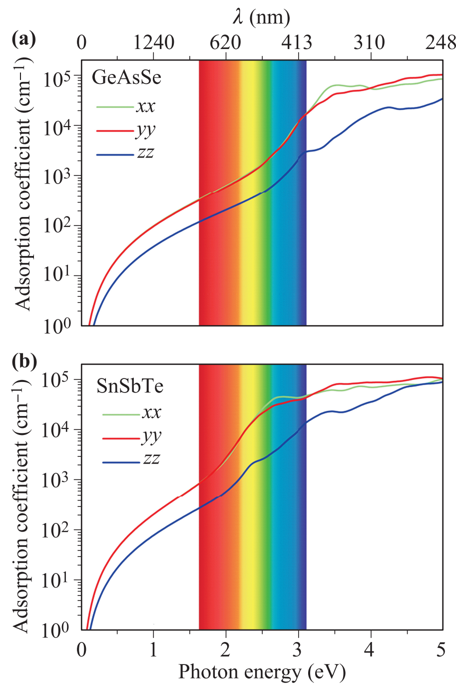

Fig. 5 Optical absorption coefficient for monolayer GeAsSe **(a)** and SnSbTe **(b)**. λ is the wave length. The area between the red and the purple represents the visible range.

where e is the electron charge; $\hbar$ is the reduced Planck constant; k_B is the Boltzmann constant; T is the temperature; m is the effective mass along the transport direction; $m_d = \sqrt{mm_\perp}$ is the average effective mass ($m_\perp$ is the effective mass perpendicular to the transport direction); and C_{2D} is the elastic modulus of the 2D sheet, which is determined by varying the lattice parameter l along the transport direction via $\Delta E/S_0 = C_{2D}(\Delta l/l)^2/2$ (ΔE is the energy change of the system under lattice deformation Δl, and S_0 is the area of the 2D sheet). $E_{1,i}$ represents the deformation potential constant of the VBM for a hole or the CBM for an electron along the transport direction, which is defined as $\Delta V/(\Delta l/l)$ (ΔV is the band edge shift under lattice deformation). All the data were calculated using a strain step of 0.5%. A room temperature value of 300 K was used in the mobility calculations. It has been demonstrated that the present scheme for computing the carrier mobility is not only computationally efficient but also physically reasonable [55, 56].

As shown in Table 2, the hole mobilities of monolayer GeAsSe and SnSbTe, which are in the range of 275.92–21 308.35 $cm^2 \cdot V^{-1} \cdot s^{-1}$, are much larger than those of electrons (17.73–92.92 $cm^2 \cdot V^{-1} \cdot s^{-1}$). Furthermore, the carrier mobility shows a rather pronounced anisotropy with a large longitudinal/horizontal ratio of up to 65, and it is thus essential to control the carrier transport directionally to enhance device performance. More importantly, the hole mobilities of these two monolayer materials are very high, approximately 20 000 $cm^2 \cdot V^{-1} \cdot s^{-1}$ for monolayer SnSbTe, which could be comparable with that of phosphorene calculated by the same method [55, 57]. Our theoretical results suggest that monolayer GeAsSe and SnSbTe should be promising candidates for 2D electronic and optoelectronic devices with highly efficient carrier transport.

The high carrier mobility of both materials can be attributed to their relatively small effective mass, large elastic modulus, and small deformation potential constant. These systems show large C_{2D} values of up to 33 $J \cdot m^{-2}$, which is comparable to that of phosphorene (29 $J \cdot m^{-2}$) [55]. The deformation potential constant $E_{1,i}$ is another important factor for carrier mobility. It reflects the strength of electron–phonon coupling and is determined by the band edge shift under lattice variation due to acoustic phonons. $E_{1,i}$ could be as low as 0.05 eV for monolayer SnSbTe (this value is much smaller than that of phosphorene, 0.15 eV), which can significantly enhance the carrier mobility. In addition to the monolayer systems, we considered bilayer GeAsSe and SnSbTe and calculated their carrier mobility. As shown in Table 2, the carrier mobility of bilayer GeAsSe and SnSbTe ranges from 13.80 to 554.03 $cm^2 \cdot V^{-1} \cdot s^{-1}$; the values are substantially smaller than those of the monolayers but comparable to those of common 2D materials such as MoS_2. The relatively high carrier mobility of bilayer systems also results from the small effective mass ($\sim 0.42 m_0$), low deformation potential constant ($\sim$0.99 eV), and large elastic modulus ($\sim$65.93 $J \cdot m^{-2}$). These results imply that layered GeAsSe and SnSbTe materials have excellent potential for use in 2D electronic devices.

Note that a recent work reported the electronic properties (band structure and carrier mobility) of monolayer GeAsSe using a 2×1 supercell [58]. After geometry optimization, however, the atomic structure of the supercell would differ from that of the 1×1 unit cell, so the electronic properties might be inaccurate. Therefore, the current calculations using a 1×1 unit cell might be more reliable. Here we further investigated the water splitting activity and optical properties of monolayer GeAsSe and SnSbTe. Our calculations indicate that both 2D materials not only have high carrier mobility but also are suitable for use as photocatalysts for water splitting, with strong absorption in the visible region.

4 Conclusion

We predicted that two new 2D semiconductors, GeAsSe and SnSbTe, possess excellent stability and various exceptional electronic properties. Monolayer GeAsSe and SnSbTe sheets are energetically favorable and have excellent dynamical and thermal stability. The relatively

weak interlayer binding energies of GeAsSe and SnSbTe indicate that both 2D monolayers could be obtained experimentally by exfoliating the corresponding bulk crystal. Importantly, monolayer GeAsSe and SnSbTe have moderate direct band gaps (2.56 and 1.96 eV, respectively) and superior hole mobility (18 150 and 21 308 $cm^2 \cdot V^{-1} \cdot s^{-1}$, respectively). The carrier mobility of the bilayer systems could be as high as 554 $cm^2 \cdot V^{-1} \cdot s^{-1}$. The calculated band gaps and band edge positions suggest that these layered materials may be suitable photocatalysts for water splitting. In particular, both monolayer GeAsSe and SnSbTe exhibit evident absorption in the visible region. All of these findings suggest that monolayer GeAsSe and SnSbTe are promising candidate materials for high-speed electronics devices, optoelectronics devices, and photocatalysis applications.

Acknowledgements This work was supported by the National Natural Science Foundation of China (Grant No. 11574040), the Fundamental Research Funds for the Central Universities of China (Grant Nos. DUT16-LAB01 and DUT17LAB19). Y. G. was supported by China Scholarship Council (CSC, Grant No. 201706060138). X. C. Z. was supported by the National Science Foundation (NSF) through the Nebraska Materials Research Science and Engineering Center (MRSEC) (Grant No. DMR-1420645). We acknowledge the computing resource from the Supercomputing Center of Dalian University of Technology and the University of Nebraska Holland Computing Center.

Appendix A Supplementary information

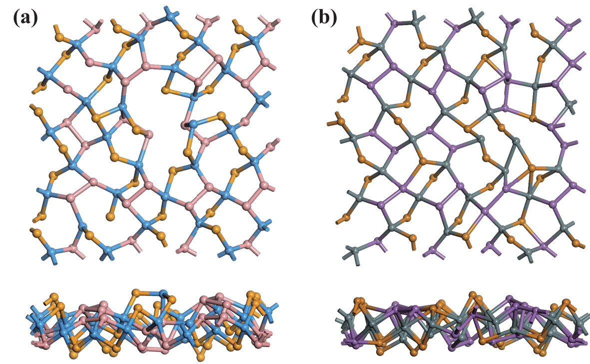

Fig. A1 Structure snapshots of **(a)** monolayer GeAsSe at 1500 K and **(b)** monolayer SnSbTe at 1000 K from BOMD simulations. Each simulation has been lasted for 10 ps.

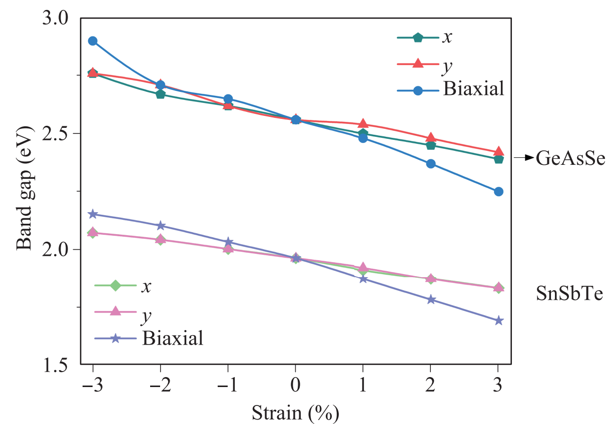

Fig. A2 Strain effect on the band gap of monolayer GeAsSe and SnSbTe based on HSE06 level.

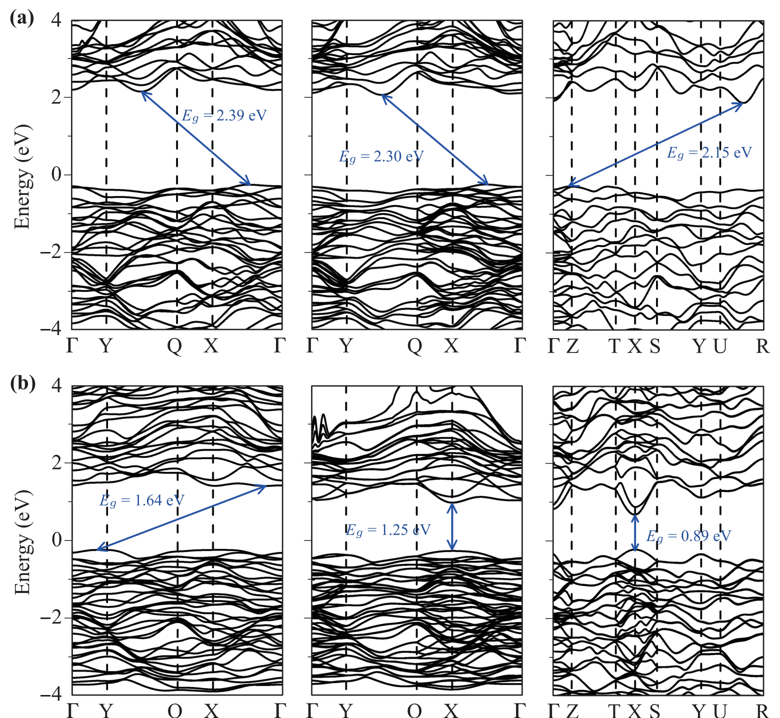

Fig. A3 Electronic band structures of **(a)** GeAsSe and **(b)** SnSbTe for bilayer (left panel), trilayer (middle panel) and bulk (right panel), respectively. E_g is the band gap denoted by the blue solid arrow. The Fermi levels are set to zero. The representation of high-symmetry points of the first Brillouin zone for bilayer and trilayer systems are illustrated in Fig. 1(c). The high-symmetry points of the first Brillouin zone for bulk systems Γ $(0, 0, 0)$, Z $(0, 0, 0.5)$, T $(-0.5, 0, 0.5)$, X $(-0.5, 0, 0)$, S $(-0.5, 0.5, 0)$, Y $(0, 0.5, 0)$, U $(0, 0.5, 0.5)$, and R $(-0.5, 0.5, 0.5)$.

References

1. K. S. Novoselov, A. K. Geim, S. V. Morozov, D. Jiang, M. I. Katsnelson, I. V. Grigorieva, S. V. Dubonos, and A. A. Firsov, Two-dimensional gas of massless Dirac fermions in graphene, *Nature* 438(7065), 197 (2005)
2. J. Zhao, H. Liu, Z. Yu, R. Quhe, S. Zhou, Y. Wang, C. C. Liu, H. Zhong, N. Han, J. Lu, Y. Yao, and K. Wu, Rise of silicene: A competitive 2D material, *Prog. Mater. Sci.* 83, 24 (2016)
3. Q. H. Wang, K. Kalantar-Zadeh, A. Kis, J. N. Coleman, and M. S. Strano, Electronics and optoelectronics of two-dimensional transition metal dichalcogenides, *Nat. Nanotechnol.* 7(11), 699 (2012)
4. L. Li, Y. Yu, G. J. Ye, Q. Ge, X. Ou, H. Wu, D. Feng, X. H. Chen, and Y. Zhang, Black phosphorus field-effect transistors, *Nat. Nanotechnol.* 9(5), 372 (2014)
5. Y. Pan, L. Zhang, L. Huang, L. Li, L. Meng, M. Gao, Q. Huan, X. Lin, Y. Wang, S. Du, H. J. Freund, and H. J. Gao, Construction of 2D atomic crystals on transition metal surfaces: Graphene, silicene, and hafnene, *Small* 10(11), 2215 (2014)
6. J. Lu, A. Carvalho, X. K. Chan, H. Liu, B. Liu, E. S. Tok, K. P. Loh, A. H. Castro Neto, and C. H. Sow, Atomic healing of defects in transition metal dichalcogenides, *Nano Lett.* 15(5), 3524 (2015)
7. M. S. Fuhrer, and J. Hone, Measurement of mobility in dual-gated MoS_2 transistors, *Nat. Nanotechnol.* 8(3), 146 (2013)
8. H. Liu, A. T. Neal, Z. Zhu, Z. Luo, X. Xu, D. Tománek, and P. D. Ye, Phosphorene: An unexplored 2D semiconductor with a high hole mobility, *ACS Nano* 8(4), 4033 (2014)
9. J. O. Island, G.A. Steele, H. S. J. v. d. Zant, and A. Castellanos-Gomez, Environmental instability of few-layer black phosphorus, *2D Mater.* 2(1), 011002 (2015)
10. A. Ziletti, A. Carvalho, D. K. Campbell, D. F. Coker, and A. H. Castro Neto, Oxygen defects in phosphorene, *Phys. Rev. Lett.* 114(4), 046801 (2015)
11. D. J. Late, B. Liu, H. S. S. R. Matte, C. N. R. Rao, and V. P. Dravid, Rapid characterization of ultrathin layers of chalcogenides on SiO_2/Si substrates, *Adv. Funct. Mater.* 22(9), 1894 (2012)
12. S. L. Li, K. Tsukagoshi, E. Orgiu, and P. Samorì, Charge transport and mobility engineering in two-dimensional transition metal chalcogenide semiconductors, *Chem. Soc. Rev.* 45(1), 118 (2016)
13. R. Fei, W. Li, J. Li, and L. Yang, Giant piezoelectricity of monolayer group IV monochalcogenides: SnSe, SnS, GeSe, and GeS, *Appl. Phys. Lett.* 107(17), 173104 (2015)
14. J. Zheng, H. Zhang, S. Dong, Y. Liu, C. Tai Nai, H. Suk Shin, H. Young Jeong, B. Liu, and K. Ping Loh, High yield exfoliation of two-dimensional chalcogenides using sodium naphthalenide, *Nat. Commun.* 5(1), 2995 (2014)
15. Y. Guo, S. Zhou, Y. Bai, and J. Zhao, Enhanced piezoelectric effect in Janus group-III chalcogenide monolayers, *Appl. Phys. Lett.* 110(16), 163102 (2017)
16. T. Gao, Q. Zhang, L. Li, X. Zhou, L. Li, H. Li, and T. Zhai, 2D ternary chalcogenides, *Adv. Opt. Mater.* 0(0), 1800058 (2018)
17. Y. Guo, S. Zhou, Y. Bai, and J. Zhao, Oxidation resistance of monolayer group-IV monochalcogenides, *ACS Appl. Mater. Interfaces* 9(13), 12013 (2017)
18. D. A. Bandurin, A. V. Tyurnina, G. L. Yu, A. Mishchenko, V. Zólyomi, S. V. Morozov, R. K. Kumar, R. V. Gorbachev, Z. R. Kudrynskyi, S. Pezzini, Z. D. Kovalyuk, U. Zeitler, K. S. Novoselov, A. Patanè, L. Eaves, I. V. Grigorieva, V. I. Fal'ko, A. K. Geim, and Y. Cao, High electron mobility, quantum Hall effect and anomalous optical response in atomically thin InSe, *Nat. Nanotechnol.* 12(3), 223 (2017)
19. Y. Guo, S. Zhou, Y. Bai, and J. Zhao, Defects and oxidation of group-III monochalcogenide monolayers, *J. Chem. Phys.* 147(10), 104709 (2017)
20. L. C. Gomes, A. Carvalho, and A. H. Castro Neto, Vacancies and oxidation of two-dimensional group-IV monochalcogenides, *Phys. Rev. B* 94(5), 054103 (2016)
21. J. Wu, C. Tan, Z. Tan, Y. Liu, J. Yin, W. Dang, M. Wang, and H. Peng, Controlled synthesis of high-mobility atomically thin bismuth oxyselenide crystals, *Nano Lett.* 17(5), 3021 (2017)
22. B. Wang, X. Niu, Y. Ouyang, Q. Zhou, and J. Wang, Ultrathin semiconducting Bi_2Te_2S and Bi_2Te_2Se with high electron mobilities, *J. Phys. Chem. Lett.* 9(3), 487 (2018)
23. J. Li, Z. Wang, Y. Wen, J. Chu, L. Yin, R. Cheng, L. Lei, P. He, C. Jiang, L. Feng, and J. He, High-performance near-infrared photodetector based on ultrathin Bi_2O_2Se nanosheets, *Adv. Funct. Mater.* 28(10), 1706437 (2018)
24. J. Wu, H. Yuan, M. Meng, C. Chen, Y. Sun, Z. Chen, W. Dang, C. Tan, Y. Liu, J. Yin, Y. Zhou, S. Huang, H. Q. Xu, Y. Cui, H. Y. Hwang, Z. Liu, Y. Chen, B. Yan, and H. Peng, High electron mobility and quantum oscillations in non-encapsulated ultrathin semiconducting Bi_2O_2Se, *Nat. Nanotechnol.* 12(6), 530 (2017)
25. X. Zhang, X. Zhao, D. Wu, Y. Jing, and Z. Zhou, $MnPSe_3$ monolayer: A promising 2D visible-light photohydrolytic catalyst with high carrier mobility, *Adv. Sci.* 3(10), 1600062 (2016)
26. X. Li, X. Wu, and J. Yang, Half-metallicity in $MnPSe_3$ exfoliated nanosheet with carrier doping, *J. Am. Chem. Soc.* 136(31), 11065 (2014)
27. C. Zha, R. Wang, A. Smith, A. Prasad, R. A. Jarvis, and B. Luther-Davies, Optical properties and structural correlations of GeAsSe chalcogenide glasses, *J. Mater. Sci. Mater. Electron.* 18(S1), 389 (2007)
28. D. T. Schaafsma, L. B. Shaw, B. Cole, J. S. Sanghera, and D. Aggarwal, Modeling of Dy^{3+}-doped GeAsSe glass 1.3-m optical fiber amplifiers, *IEEE Photonics*

Technol. Lett. 10(11), 1548 (1998)

29. A. Zakery, and M. Hatami, Nonlinear optical properties of pulsed-laser-deposited GeAsSe films and simulation of a nonlinear directional coupler switch, *J. Opt. Soc. Am. B* 22(3), 591 (2005)
30. N. Ashok, Y. L. Lee, and W. Shin, GeAsSe chalcogenide slot optical waveguide ring resonator for refractive index sensing, in: 2017 25th Optical Fiber Sensors Conference (OFS), 2017
31. F. Hulliger and T. Siegrist, The crystal structure of GeAsSe, *Mater. Res. Bull.* 16(10), 1245 (1981)
32. J. H. Yang, Y. Zhang, W. J. Yin, X. G. Gong, B. I. Yakobson, and S. H. Wei, Two-dimensional SiS layers with promising electronic and optoelectronic properties: Theoretical prediction, *Nano Lett.* 16(2), 1110 (2016)
33. E. Ziambaras, J. Kleis, E. Schröder, and P. Hyldgaard, Potassium intercalation in graphite: A van der Waals density-functional study, *Phys. Rev. B* 76(15), 155425 (2007)
34. R. Zacharia, H. Ulbricht, and T. Hertel, Interlayer cohesive energy of graphite from thermal desorption of polyaromatic hydrocarbons, *Phys. Rev. B* 69(15), 155406 (2004)
35. G. Kresse and J. Furthmüller, Efficient iterative schemes for ab initio total-energy calculations using a plane-wave basis set, *Phys. Rev. B* 54(16), 11169 (1996)
36. G. Kresse and D. Joubert, From ultrasoft pseudopotentials to the projector augmented-wave method, *Phys. Rev. B* 59(3), 1758 (1999)
37. J. P. Perdew, K. Burke, and M. Ernzerhof, Generalized gradient approximation made simple, *Phys. Rev. Lett.* 77(18), 3865 (1996)
38. H. J. Monkhorst and J. D. Pack, Special points for Brillouin-zone integrations, *Phys. Rev. B* 13(12), 5188 (1976)
39. J. Heyd, G. E. Scuseria, and M. Ernzerhof, Hybrid functionals based on a screened Coulomb potential, *J. Chem. Phys.* 118(18), 8207 (2003)
40. S. Grimme, Semiempirical GGA-type density functional constructed with a long-range dispersion correction, *J. Comput. Chem.* 27(15), 1787 (2006)
41. L. A. Burns, Á. V. Mayagoitia, B. G. Sumpter, and C. D. Sherrill, Density-functional approaches to noncovalent interactions: A comparison of dispersion corrections (DFT-D), exchange-hole dipole moment (XDM) theory, and specialized functionals, *J. Chem. Phys.* 134(8), 084107 (2011)
42. S. Baroni, S. de Gironcoli, A. Dal Corso, and P. Giannozzi, Phonons and related crystal properties from density-functional perturbation theory, *Rev. Mod. Phys.* 73(2), 515 (2001)
43. R. N. Barnett and U. Landman, Born-Oppenheimer molecular-dynamics simulations of finite systems: Structure and dynamics of $(H_2O)_2$, *Phys. Rev. B* 48(4), 2081 (1993)
44. G. J. Martyna, M. L. Klein, and M. Tuckerman, Nosé–Hoover chains: The canonical ensemble via continuous dynamics, *J. Chem. Phys.* 97(4), 2635 (1992)
45. M. D. Segall, R. Shah, C. J. Pickard, and M. C. Payne, Population analysis of plane-wave electronic structure calculations of bulk materials, *Phys. Rev. B* 54(23), 16317 (1996)
46. L. Zhou, Y. Guo, and J. Zhao, GeAs and SiAs monolayers: Novel 2D semiconductors with suitable band structures, *Physica E* 95, 149 (2018)
47. V. Chakrapani, J. C. Angus, A. B. Anderson, S. D. Wolter, B. R. Stoner, and G. U. Sumanasekera, Charge transfer equilibria between diamond and an aqueous oxygen electrochemical redox couple, *Science* 318(5855), 1424 (2007)
48. H. L. Zhuang and R. G. Hennig, Single-layer group-III monochalcogenide photocatalysts for water splitting, *Chem. Mater.* 25(15), 3232 (2013)
49. Z. Ma, J. Zhuang, X. Zhang, and Z. Zhou, SiP monolayers: New 2D structures of group IV–V compounds for visible-light photohydrolytic catalysts, *Front. Phys.* 13(3), 138104 (2018)
50. X. Zhang, Z. Zhang, D. Wu, X. Zhang, X. Zhao, and Z. Zhou, Computational screening of 2D materials and rational design of heterojunctions for water splitting photocatalysts, *Small Methods* 2(5), 1700359 (2018)
51. A. R. Beal and H. P. Hughes, Kramers-Kronig analysis of the reflectivity spectra of 2H-MoS_2, 2H-$MoSe_2$ and 2H-$MoTe_2$, *J. Phys. C Solid State Phys.* 12(5), 881 (1979)
52. S. Takagi, A. Toriumi, M. Iwase, and H. Tango, On the universality of inversion layer mobility in Si MOSFET's: Part I-effects of substrate impurity concentration, *IEEE Trans. Electron Dev.* 41(12), 2357 (1994)
53. S. Bruzzone and G. Fiori, Ab-initio simulations of deformation potentials and electron mobility in chemically modified graphene and two-dimensional hexagonal boron-nitride, *Appl. Phys. Lett.* 99(22), 222108 (2011)
54. G. Fiori and G. Iannaccone, Multiscale modeling for graphene-based nanoscale transistors, *Proc. IEEE* 101(7), 1653 (2013)
55. J. Qiao, X. Kong, Z. X. Hu, F. Yang, and W. Ji, High-mobility transport anisotropy and linear dichroism in few-layer black phosphorus, *Nat. Commun.* 5(1), 4475 (2014)
56. J. Dai and X. C. Zeng, Titanium trisulfide monolayer: Theoretical prediction of a new directg semiconductor with high and anisotropic carrier mobility, *Angew. Chem. Int. Ed.* 127(26), 7682 (2015)
57. Y. Guo, S. Zhou, J. Zhang, Y. Bai, and J. Zhao, Atomic structures and electronic properties of phosphorene grain boundaries, *2D Mater.* 3(2), 025008 (2016)
58. W. Zhang, Y. G. Wang, Y. Ding, J. Yin, and P. Zhang, Two-dimensional GeAsSe with high and unidirectional conductivity, *Nanoscale* (2018)